Automated multi-objective and multidisciplinary design optimization of a transonic turbine stage

L Song, C Luo, J Li, and **Z Feng***
Institute of Turbomachinery, Xi'an Jiaotong University, Xi'an, People's Republic of China

The manuscript was received on 1 March 2011 and was accepted after revision for publication on 8 September 2011.

DOI: 10.1177/0957650911425005

Abstract: An automated multi-objective and multidisciplinary design optimization (MDO) of a transonic turbine stage to maximize the isentropic efficiency and minimize the maximum stress of the rotor with constraints on mass flowrate and dynamic frequencies is presented in this article. The self-adaptive multi-objective differential evolution (SMODE) algorithm is studied and developed to seek Pareto solutions of the optimization, and a new constraint-handling method based on multi-objective optimization concept is applied for constraint handling. The optimization performance of the presented SMODE is demonstrated using the typical mathematical tests. By applying SMODE as an optimizer and integrating three-dimensional (3D) blade modelling method based on non-uniform B-spline, load-fitting transfer algorithm in parameter space, 3D Navier–Stokes solution technique, and finite element analysis method as well, seven Pareto solutions are obtained. Two Pareto solutions are analysed in detail. One is the highest isentropic efficiency individual, while the other is a compromise between efficiency and mechanical stress in the blade. The aerodynamic performance and strength characteristics of the optimized turbine stage are significantly improved. The analysis results indicate that the presented multi-objective and MDO method has a potential in the optimization of blade performance and can be applied as a promising method for the optimization design of axial turbomachinery blades

Keywords: multidisciplinary design optimization, multi-objective differential evolution algorithm, turbine stage

1 INTRODUCTION

The automated optimization design of three-dimensional (3D) turbine blades belongs to the typical aerodynamic designs [**1–3**]. However, the obtained 3D blade geometrics with high aeroperformance are usually not acceptable in the structural design process, which is especially true for high-rotational speed rotors. A satisfactory blade geometry usually needs several iterations between the aero-optimization and the structure analysis. Therefore, an automated optimization design method should be established in order to obtain a bilaterally satisfying compromise between high aeroperformance and structural reliability.

Nowadays, multidisciplinary design optimization (MDO) methods, using the idea of parallel synergy design and integrated manufacturing techniques, have attracted much attention from the field of turbomachinery, and a few automated MDO methods for turbomachinery blades have been developed. Moroz *et al.* [**4**] used the design of experiment method and reduced-order models for design optimization of axial turbine blades to achieve stage maximal efficiency meeting both stress–strain and vibration reliability requirements. Verstraete *et al.* [**5**] combined a genetic algorithm with an artificial neural network (ANN) to optimize a radial compressor for microgas turbine application, using a 3D Navier–Stokes and a finite element method (FEM) analysis technology. Pierret *et al.* [**6**] conducted an automated multidisciplinary optimization of the

**Corresponding author: Institute of Turbomachinery, School of Energy and Power Engineering, Xi'an Jiaotong University, Xi'an 710049, People's Republic of China.*
email: zpfeng@mail.xjtu.edu.cn

NASA Rotor 67 using a genetic algorithm that took into account physics aspects such as aeromechanics both static and dynamic. Siller *et al.* [**7**] performed an automated multidisciplinary optimization design of an axial transonic compressor using an evolutionary algorithm combined with a Kriging model and an ANN, and the results showed that the aerodynamic efficiency and the strength performance of the compressor were significantly improved.

Despite a few automated MDO methods which have been already developed for turbomachinery blade, research reported on multi-objective and multidisciplinary optimization of blades is insufficient. In the practical engineering application, sometimes one wants to obtain the blades which have both high efficiency and low stress. This is because the lower the stress of the blades is, the longer the lifetime of the blades may be, and that the blades can be manufactured using the low-price material, which will reduce the manufacturing cost. In order to obtain the blades with high efficiency and low stress, one needs to choose the stress as the second objective for optimization. On the other hand, many Pareto solutions can be obtained by choosing the stress as the second objective, and the designers can choose the appropriate solution according to the practical engineering requirements. Hence, it is necessary to do some more detailed investigation into the stress as the second objective to satisfy the practical engineering application requirements.

In this study, an algorithm named 'self-adaptive multi-objective differential evolution (SMODE)' is first proposed, and tests conducted on multi-objective mathematical functions demonstrated a good performance in both global convergence and distribution compared with the NSGA-II and SPEA2 algorithms. Subsequently, SMODE is applied as an optimizer to find the Pareto solution sets of multi-objective design problems, and an automated multi-objective and MDO method for turbomachinery blades is developed. To validate the optimization capability of this method, a transonic turbine stage is optimized to maximize the isentropic efficiency and minimize the maximum stress in the rotor with constraints on mass flowrate and dynamic frequencies. The aerodynamic and mechanical performance of the obtained Pareto designs are discussed and compared with those of the reference design in detail.

2 SMODE ALGORITHMS

2.1 Algorithm description

Differential evolution (DE) is a new evolution algorithm first proposed by Storn and Price [**8**, **9**] in 1995. In the single-objective optimization, DE is simpler in structure, better in robustness, and faster in convergence than other evolution algorithms. Owing to these advantages of DE, some researchers have tried to further develop it to solve multi-objective optimization problems [**10–12**]. Based on the self-adaptive mechanism from evolution strategies, Pareto-based ranking, and crowding distance sorting, a SMODE algorithm is developed and proposed in this study. The flow chart of this algorithm is shown in Fig. 1 and described as follows.

1. Input: Multi-objective optimization problem (*MOP*), Maximum generation (*MAXGEN*), Population size (*NP*), Dimension of problem (*D*), Scaling factor (*F*), and Crossover factor (*CR*).
2. Randomly generate initial population which includes *NP* individuals.
3. Evaluate the initial population, and perform the fast non-dominated sorting of the initial population.
4. Select the new population which includes *NP* individuals from the initial population by adopting the tournament selection method according to the Pareto-based ranking of individuals in the initial population, and then use the new population as the parent population.

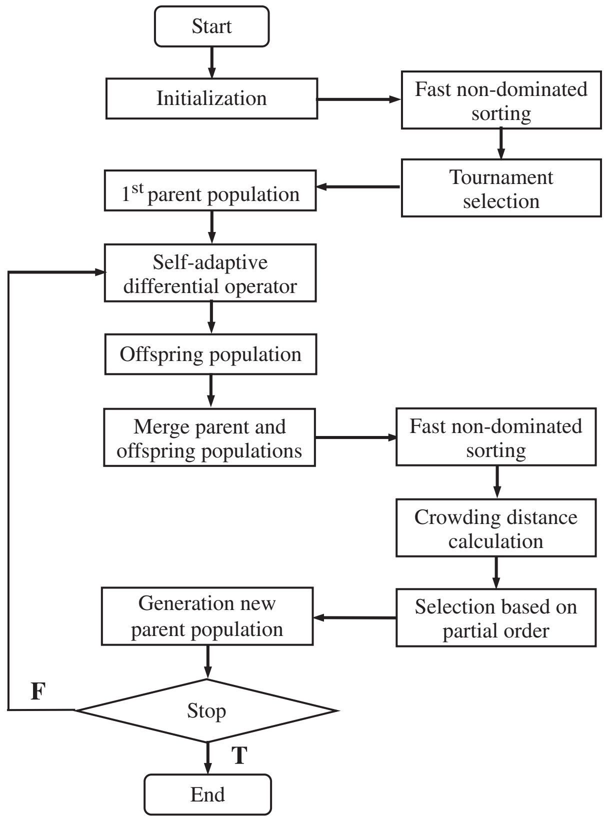

Fig. 1 Flow chart of the SMODE

5. Carry out the self-adaptive differential operation on the parent population in order to generate the offspring population.

   5.1. Select three individuals $X_{r1,i}$, $X_{r2,i}$, and $X_{r3,i}$ from the parent population using the tournament selection method, where $r1$, $r2$, and $r3$ are pairwise different, and then generate a new individual by the mutation and crossover operations. The self-adaptive mechanism from evolution strategies [**12**, **13**] is applied to the differential operation, and scaling factor F and crossover factor CR will be adjusted to the appropriate values during the evolutionary process. The specific implemented processes are as follows.

   First, the ith individual's encoding $\{x_{1i,g}, x_{2i,g}, \ldots, x_{Di,g}\}$ is extended to $\{x_{1i,g}, x_{2i,g}, \ldots, x_{Di,g}, F_{i,g}, CR_{i,g}\}$. In the initialization, both F and CR values of each individuals are initialized. Then, the average values $\overline{F}_{g,i}$ and $\overline{CR}_{g,i}$ of each individual are calculated as follows

$$\overline{F}_{g,i} = (F_{i,g} + F_{r1,g} + F_{r2,g} + F_{r3,g})/4 \qquad (1)$$

$$\overline{CR}_{g,i} = (CR_{i,g} + CR_{r1,g} + CR_{r2,g} + CR_{r3,g})/4 \qquad (2)$$

   The $F_{i,g+1}$ value of the ith individual in the gth generation is calculated by the following equation

$$F_{i,g+1} = \overline{F}_{g,i} \times e^{\tau\cdot(-|N(0,1)|)} \qquad (3)$$

   where $N(0,1)$ denotes a random number with the normal distribution, $|N(0,1)|$ the absolute value of the random number, and τ a constant defined as $MAXGEN/3$.

   The ith candidate of the next generation is generated by mutation. It is formulated as follows

$$V_{i,g+1} = X_{r1,g} + F_{i,g+1} \cdot (X_{r2,g} - X_{r3,g}) \qquad (4)$$

   The following formula is used for calculating the $CR_{i,g+1}$ value of the ith individual in the gth generation

$$CR_{i,g+1} = \overline{CR}_{g,i} \times e^{\frac{N(0,1)}{8\sqrt{2D}}} \qquad (5)$$

   The crossover operation is conducted as follows

$$\hat{u}_{ji,g+1} = \begin{cases} v_{ji,g+1} & if\ randb \leqslant CR_{i,g+1}\ or\ j = randr \\ x_{ji,g} & otherwise \end{cases}$$
$$i = 1, \ldots, NP, \qquad j = 1, \ldots, D \qquad (6)$$

   5.2. Li and Zhang [**14**] found that the polynomial mutation can facilitate to improve the optimization performance of DE. Thus, here the polynomial mutation to the multi-objective DE is applied as follows

$$u_{ji,g+1} = \begin{cases} \hat{u}_{ji,g+1} + \tau_{ji,g+1} \times (UP_j - LOW_j) & randm < P_m \\ \hat{u}_{ji,g+1} & randm \geqslant P_m \end{cases} \qquad (7)$$

$$\tau_{ji,g+1} = \begin{cases} (2 \times randk)^{\frac{1}{\eta+1}} - 1 & randk < 0.5 \\ 1 - (2 - 2 \times randk)^{\frac{1}{\eta+1}} & randk \geqslant 0.5 \end{cases} \qquad (8)$$

   where both $randm$ and $randk$ are randomized numbers from $[0, 1]$, P_m the mutation rate, η the distribution index, and UP_j and LOW_j the upper and lower bounds of the jth decision variable, respectively.

   5.3. Repair: When $u_{ji,g+1}$ is greater than the upper bound, its value is set to be equal to the upper bound. When $u_{ji,g+1}$ is smaller than the lower bound, its value is set to be equal to the lower bound.

6. Evaluate the offspring population. A mating pool is created by combining the parent and offspring populations, and fast non-dominated sorting and crowding distance estimation for the mating pool are completed.
7. Select the best NP individuals from the mating pool according to the partial order relationship between the individuals, and then use them to replace the parent population.
8. Finish the optimization design process when the stopping criterion is satisfied. Otherwise go to Step 4 to continue the optimization procedure.

2.2 Constraint-handling approaches and functional tests

As many practical problems are constrained multi-objective problems in scientific research studies and engineering practices, it is essential to investigate the constraint-handling approaches for multi-objective optimization. At present, most constraint-handling approaches can be divided into two classes. One is the penalty function method and the other is the constraint-handling approach based on multi-objective optimization concept. Penalty function method is widely applied to solve practical problems. However, this method strongly depends on the penalty factors, and has to be carefully tuned to obtain a satisfactory solution for every optimization problem. If the penalty factors are too small, the optimized solution might not satisfy the constraints. On the other hand, if the penalty factors are too large, it would be difficult to obtain a satisfactory objective function value.

Thus, a great number of constraint-handling approaches based on multi-objective optimization

Table 1 Constrained test problems

Problem	Variable bounds	Objective functions	Constraints
SRN	$x=[-20,20]^2$	$f_1(x)=(x_1-2)^2+(x_2-1)^2+2$ $f_2(x)=9x_1-(x_2-1)^2$	$g_1(x)=x_1^2+x_2^2\leqslant 225$ $g_2(x)=x_1-3x_2\leqslant -10$
TNK	$x=[0,\pi]^2$	$f_1(x)=x_1$ $f_2(x)=x_2$	$g_1(x)=-x_1^2-x_2^2+1+$ $0.1\cos(16\arctan(x_1/x_2))\leqslant 0$ $g_2(x)=(x_1-0.5)^2+$ $(x_2-0.5)^2\leqslant 0.5$
OSY	$x_{1,2,6}=[0,10]^3$ $x_{3,5}=[1,5]^2$ $x_4=[0,6]$	$f_1(x)=-(25(x_1-2)^2+(x_2-2)^2+$ $(x_3-1)^2+(x_4-4)^2+$ $(x_5-1)^2)$ $f_2(x)=x_1^2+x_2^2+x_3^2+x_4^2+x_5^2+x_6^2$	$g_1(x)=2-x_1-x_2\leqslant 0$ $g_2(x)=x_1+x_2-6\leqslant 0$ $g_3(x)=x_2-x_1-2\leqslant 0$ $g_4(x)=x_1-3x_2-2\leqslant 0$ $g_5(x)=(x_3-3)^2+x_4-4\leqslant 0$ $g_6(x)=4-(x_5-3)^2-x_6\leqslant 0$

concept [**15–17**] have been proposed to handle constrained optimization problems without tuning the penalty factors. These approaches usually divide the two solutions to be compared into three cases. The first case is that the two solutions are both feasible. The second case is that one is feasible and the other is not. The third is that neither of the two is feasible. For the first case, the two solutions are compared in the objective function space to determine the dominant relationship. For the second case, the criterion that the feasible one is superior to the infeasible one proposed by Jimenez and Verdegay [**18**] is generally adopted. The main difference between these constraint-handling approaches based on multi-objective optimization concept is reflected in the third case. In practical engineering application, since the characteristic that the evaluation time of objective function is much more than the numerical calculation time in algorithms, a constraint-handling approach based on multi-objective optimization concept is developed in this study as follows.

Definition 1: If any of the following conditions is satisfied, a solution u is said to be a constrained-dominate solution v.

1. Solutions u and v are both feasible solutions, and solution u dominates solution v in the objective function space.
2. Solution u is feasible and solution v is not.
3. Solutions u and v are both infeasible and solution u dominates solution v in the constraint space.
4. Solutions u and v are both infeasible solutions. There is no dominated relationship between solutions u and v in the constraint space, but the total amount of constraint violation of solution u is smaller than that of solution v. The constraint violations of both mass flowrate and dynamic frequencies are needed to be non-dimensionalized. Where the total amount of constraint violation for an individual $\vec{x}$ is calculated by

$$coef\,(\vec{x})=\sum_{n=1}^{n_{\max}}\max(g_n(\vec{x}),0) \tag{9}$$

In the third item mentioned above, dominance in constraint space is defined as follows.

Definition 2: If the following two solutions are both true, solution u is said to be a dominate solution v in the constraint space.

All constraints of solution u is no worse than that of solution v

$$G_i(u)\leqslant G_i(v),\quad i=1,2,\ldots,p \tag{10}$$

The least one constraint of solution u is strictly better than that of solution v

$$\exists j\in\{1,2,\ldots,p\},\ G_j(u)<G_j(v) \tag{11}$$

where

$$G_i(x)=\max(0,g_i(x))$$

To verify the performance of this proposed constraint-handling approach, three typical constrained multi-objective problems (Table 1) are chosen. In all problems, one uses a population size of 100, and run SMODE with the proposed constraint-handling approach for a maximum of 500 generations. The real coding is adopted. The initial values of scaling factor F and crossover factor CR are set to be 0.45 and 0.75, respectively, and the mutation probability and the distribution index are defined as $1/n$ and 50, respectively. Figures 2 to 4 give the obtained non-dominated solutions on different test problems. These figures indicate that all the obtained non-

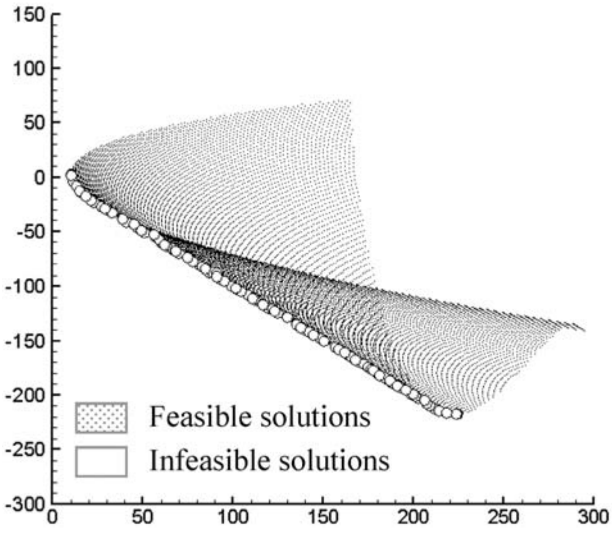

Fig. 2 Obtained non-dominated solutions on SRN

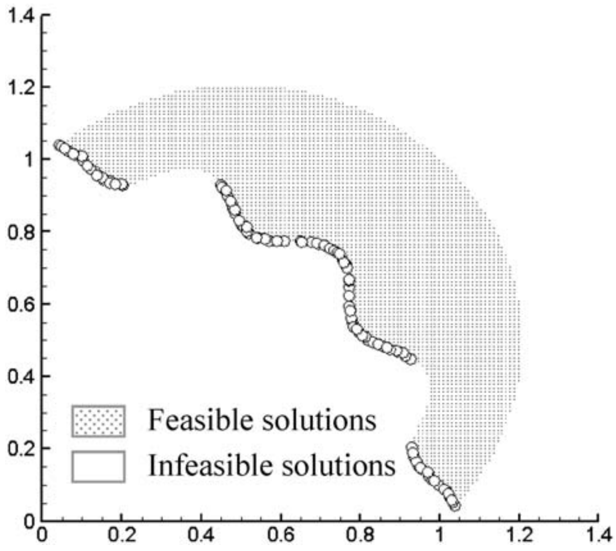

Fig. 3 Obtained non-dominated solutions on TNK

dominated solutions converge to the Pareto-optimal frontiers, and the distributions of the obtained non-dominated solutions are remarkably uniform. The results imply that the presented SMODE can effectively solve the multi-constraint and multi-objective problems.

3 MULTI-OBJECTIVE AND MDO METHOD OF AXIAL TURBOMACHINERY BLADES

A multi-objective and MDO method of axial turbomachinery blades is proposed, in which one applies SMODE as an optimizer and combine all together 3D blade modelling method based on non-uniform B-spline, load-fitting transfer algorithm in parameter space, 3D Navier–Stokes solution technique, and

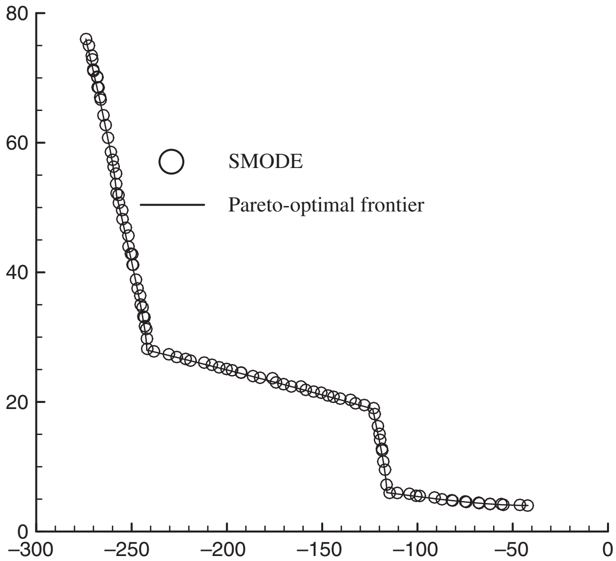

Fig. 4 Obtained non-dominated solutions on OSY

finite element analysis method. Figure 5 shows the flowchart of this method.

4 APPLICATION OF MDO TO TRANSONIC TURBINE STAGE

4.1 Description of the problem

With the development of high-performance and high-load turbomachinery, transonic blades are widely employed in both turbine and compressor stages. Here, the application of MDO to a steam turbine transonic stage is conducted. Compared with the optimization of subsonic turbine stage, the optimization of the transonic turbine stage is a more challenging work. The stator of the turbine stage is a straight blade and the rotor is a twisted one. Table 2 gives the geometrical parameters and corresponding flow boundary condition.

4.2 Performance evaluation of varied disciplines

To evaluate the aerodynamic performance of the transonic turbine stage, the Reynolds-averaged Navier–Stokes equations are applied in the present simulation using commercial software NUMECA Euranus [**19**]. The Spalart–Allmaras turbulence model is used to simulate the turbulent flow. A finite volume method is adopted for spatial discretization, and the numerical scheme is a centre difference scheme. The four-step Runge–Kutta algorithm is used to ensure numerical time integration. An implicit residual smoothing phase is utilized to obtain high Courant–Friedrichs–Lewy (CFL) number.

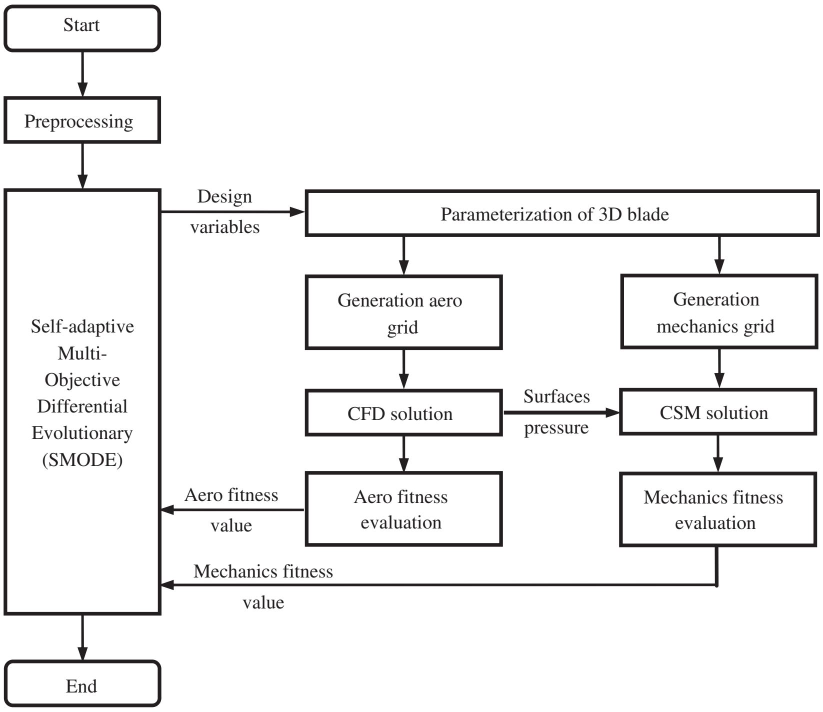

Fig. 5 Flow chart of the multi-objective and MDO method

Table 2 Parameters of the transonic turbine stage

Parameters	Stator	Rotor
Number of blades	58	90
Blade height (mm)	203	238
Diameter of blade root (mm)	1.905	1.905
Rotor speed (rpm)	0	3000
Inlet total temperature (K)	487.22	—
Inlet total pressure (Pa)	235 184.3	—
Outlet static pressure (Pa)	—	95 000

The Default grid structure of NUMECA AutoGrid5 is adopted for meshing of blade, and the size of the first cell to wall is set to 0.008 mm. Before the optimization, the grid-independent analysis of computational fluid dynamics calculation is performed, in which three different density grids are selected. The node number distributions in B2B planes of Grids 1 and 2 are shown in Fig. 6. The node numbers of Grids 1 and 2 in the span are both 49. The node number distribution in B2B plane of Grid 3 is the same as that of Grid 2, and the difference lies in the fact that the node number of Grid 3 in the span is 65. Table 3 presents the numbers of grid cells and the aerodynamic calculation results of different grids. As can be seen from this table, both the mass flowrate and isentropic efficiency of the three different grids have very small differences. In addition, considering that the relative aerodynamic performance values of the different design candidates in the same grid are mainly concerned over the optimization, Grid 1 with the smallest density (Fig. 7) is adopted in the MDO to reduce the optimization time.

In the MDO process of the turbine stage, the evaluations of the strength and vibration characteristics are aimed at the rotor of the turbine stage. The maximum von Mises stress and the vibration frequencies of rotor are calculated using commercial software ANSYS 11.0 [**20**]. Ten-node tetrahedral elements are used as a compromise between element quality and automatic meshing. The automated modelling with a fillet for each candidate blade is a very difficult problem, which cannot be realized in the current conditions, so one does not consider a fillet radius between blade and hub (Fig. 8). The computational highest stress without a fillet radius between blade and hub may be not the actual maximum stress, but the relative size of the highest stress of the different candidate blades can be reflected. The centrifugal forces and the fluid pressure are imposed on the FEM computation. The highest stress of the blade, which excludes the hub, is mainly considered in this article, so not a contact surface but the fixed displacement boundary conditions are imposed on this fir tree to reduce the computing time. To separate aerodynamic and structural analysis meshes, a load surface method [**21**] is used to transfer the pressure of blade surfaces. Table 4 shows the material properties and safety factor of the rotor.

4.3 Design variables and objectives

The non-uniform B-spline is adopted to parameterize turbine stage blades. Considering that the stator is a

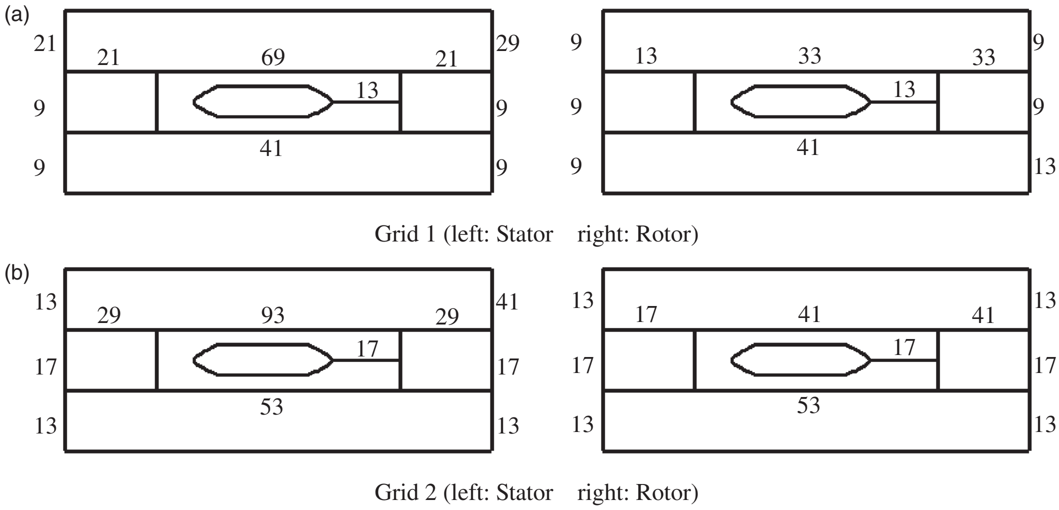

Fig. 6 The node number distributions in B2B planes of the different grids: (a) Grid 1 (left: stator and right: rotor) and Grid 2 (left: stator and right: rotor)

Table 3 The numbers of grid cells and the aerodynamic calculation results of different grids

	Number of grid cells of stator	Number of grid cells of rotor	The total number of grid cells	Mass flowrate (kg/s)	Isentropic efficiency
Grid 1	225 449	157 437	382 886	125.63	0.9469
Grid 2	437 129	291 697	728 826	125.54	0.9480
Grid 3	579 865	386 945	966 810	125.46	0.9478

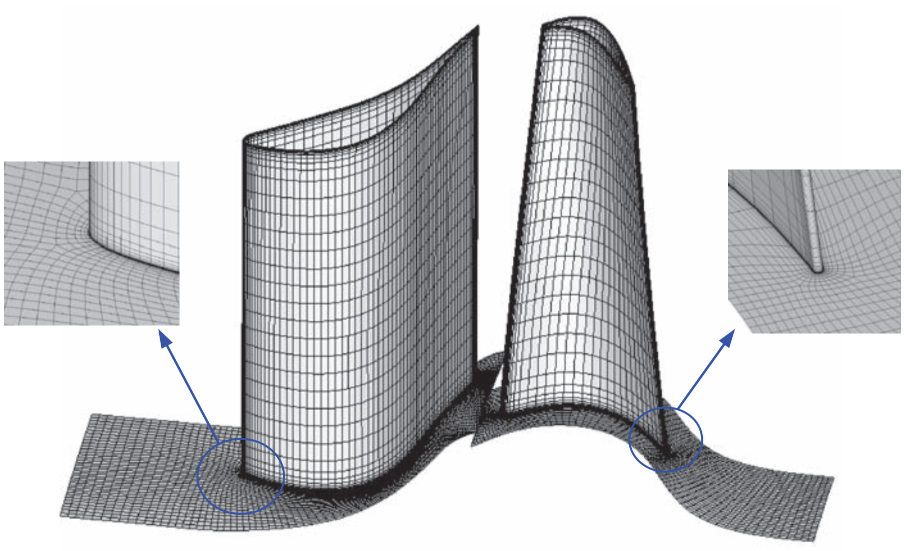

Fig. 7 Aerodynamic computation grid in MDO of the turbine stage

straight blade, the stator parameterization is mainly conducted in two aspects: two-dimensional section profile and lean mode, in order to form a leaned blade with a uniform section. The root section of the stator is selected as the datum plane, and is defined by five active control points on the suction surface. The middle and tip sections are consistent with the datum plane, and are both defined only by a circumferential translation parameter. The circumferential translation parameter transfers the chosen section along the circumferential direction, and is used to control the lean of the blade. The rotor is a twisted blade, and is parameterized by the root, middle, and tip sections. The root section is defined by five active control points on the suction surface. The middle and tip sections are defined by four active

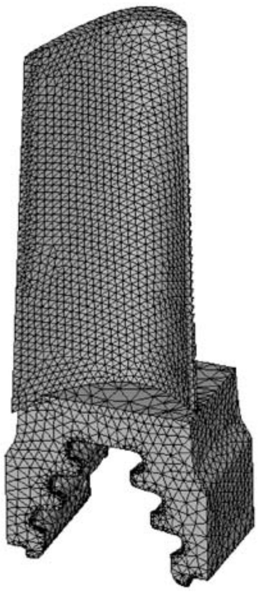

Fig. 8 FEM analysis grid in MDO of the turbine stage

Table 4 Material properties and safety factor

Parameters	Value or name
Material	1Cr12Ni2W1Mo1V
Elasticity modulus (GPa)	202.8
Poisson ratio	0.3
Mass density (kg/m $^{3)}$	7.840
Limiting strength (MPa)	735
Safety factor	1.7

control points and one circumferential translation parameter, respectively (Fig. 9).

To reduce the dimension of the search space, the above active control points are only varied along the normal direction. Every active control point can be described by only one parameter. The stator is controlled by 7 design variables, and the rotor is controlled by 15 design variables. Thus, 22 design variables in total are adopted for the MDO of the turbine stage.

The turbine stage is optimized to maximize the isentropic efficiency and minimize the maximum stress in the rotor with constraints on mass flow and dynamic frequencies of the rotor. The vibration frequencies on the fixed rotational speed are primarily concerned with, so the Campbell diagram is not analysed in this article. The constraint on dynamic frequencies of the rotor will be specifically described in the following.

In general, the rotor is required to avoid two kinds of exciting frequencies. One is the high-frequency excitation caused by the stator trailing-edge wake, which is defined as $f_{e,h} = KZ_1 n_s,\ \ K = 1, 2, 3,$ where Z_1 is the number of stator blades and n_s the rotational speed of the rotor per second. The other is the low-frequency excitation caused by the rotation of rotor in the non-uniform airflow, which is defined as $f_{e,l} = Kn_s,\ \ K = 1, 2, 3, \ldots, 6$. In the MDO process of the turbine stage in this article, as the first dynamic frequency of the rotor is much higher than the first six low-frequency excitations, avoiding the high-frequency excitation will be mainly considered. The margins which are imposed to the first three high-frequency excitations are set to be ±12 per cent, ±7 per cent, and ±5 per cent, respectively. This imposition results in the following forbidden ranges: 2552–3248, 5394–6206, and 8265–9135 Hz. Then, the first to tenth vibration frequencies of the rotor are excluded from these ranges. The excitation frequencies obtained by a steady-state approach may have deviations from the practical excitation frequencies. However, under the current calculation conditions, carrying out the optimization of the 3D turbine stage based on unsteady approach is unrealistic, which will spend huge time and is difficult to be applied to practical engineering design optimization. The analysis of the vibration frequencies of blades is simplified. The temperature-weakening effect and the interference between adjacent blades are also not taken into account in this study, and the validity of the results is restricted within the limits of the hypotheses in this article. In the future, under the more mature condition, one will improve the calculation accuracy of the excitation frequencies to satisfy the engineering actual requirements more. Especially, one will adopt the unsteady flow simulation method for optimization, this is because the unsteady rotor–stator interaction [**22**, **23**] has a great influence on the performances of the turbine stage.

Thus, the mathematical expression of the objective function is as follows

$$
\begin{aligned}
&\max\ F_{obj}(\gamma) = [\eta_{is}(\gamma),\ -\sigma_{\max}(\gamma)] \\
&\textit{subject to} \\
&\qquad 0.98 \cdot m_{ref} \leqslant m \leqslant 1.02 \cdot m_{ref} \\
&\quad f_{j,vib} \notin \left[f_{i,forb}^{low}, f_{i,forb}^{up} \right], \\
&\quad j = 1, 2, 3, \ldots, 10, \qquad i = 1, 2, 3.
\end{aligned}
\tag{12}
$$

where the isentropic efficiency of the turbine stage is calculated by

$$
\eta_{is} = \frac{h_{01} - h_{02}}{h_{01} - h_{02}^{is}} \tag{13}
$$

where h_{01} denotes the inlet total enthalpy of the turbine stage, h_{02} the outlet total enthalpy, and h_{02}^{is} the ideal enthalpy value corresponding to the outlet total pressure of the turbine stage.

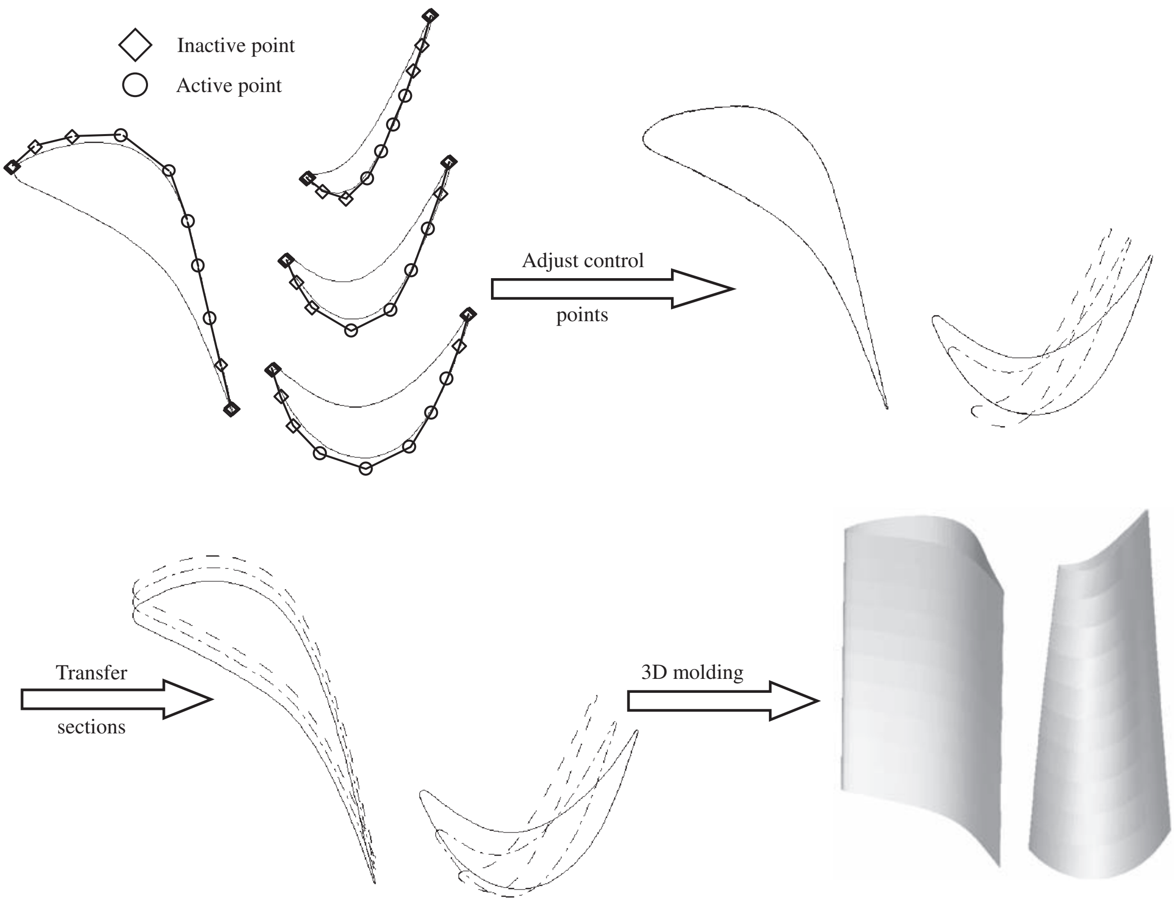

Fig. 9 Parameterization process of the turbine stage

5 RESULTS AND DISCUSSION

In the MDO process of the turbine stage, both the population size and the maximum generation are set to be 60. It takes about 100 min to evaluate the aerodynamic performance for each individual, and it takes about 8 min to conduct the FEM computational for each individual. Coarse-grained parallel strategy with ten CPUs (3.0 GHz) is applied to speed up the optimization process. It took about 27 days for the 60×60 evaluations. After the optimization, seven Pareto solutions were obtained. Hereby, Design A with the optimal isentropic efficiency of the turbine stage and design B with the good aeroperformance and low-stress turbine stage are selected for special analysis (Fig. 10).

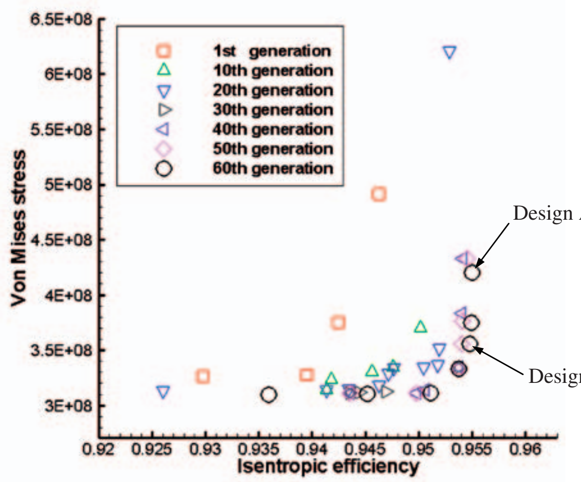

Fig. 10 Optimization results with convergence history

The configurations of the Pareto solutions design A and design B are compared with the reference design at different sections in Fig. 11. As can be seen from the profiles at the root section, the profiles of designs A and B are very close to each other. In front of the throat of the suction-side surface, the curvature of the optimized stators decreases compared with reference stator. In rear of the throat of the suction-side surface, the profiles of the optimized stators are closer to a straight line. The trailing edge turning angles of the optimized stators are reduced. Compared with the reference rotor, all curvatures of the optimized rotors at the suction-side surface increase. As can be seen from the profiles in the middle section, compared with the reference stage, the circumferential

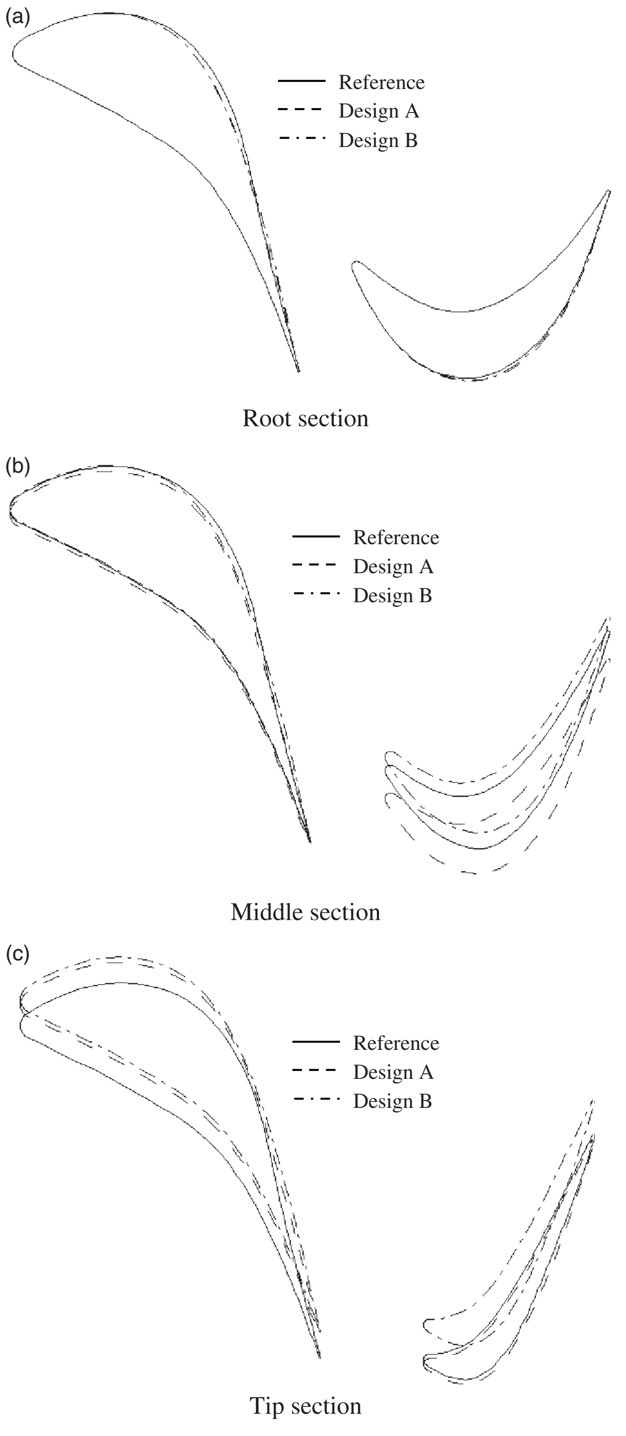

Fig. 11 Comparison between the profiles of the reference design and optimized designs: (a) root section, (b) middle section, and (c) tip section

translation of the optimized stators is not obvious, whereas the rotor of Design A shows an apparent translation along the rotational direction, and the rotor of Design B transfers along the direction opposite to the rotational direction. In the tip section, the optimized stators translate obviously along the suction-side surfaces, and form a positive bowed design at the top of the stator; the rotor of Design A has little

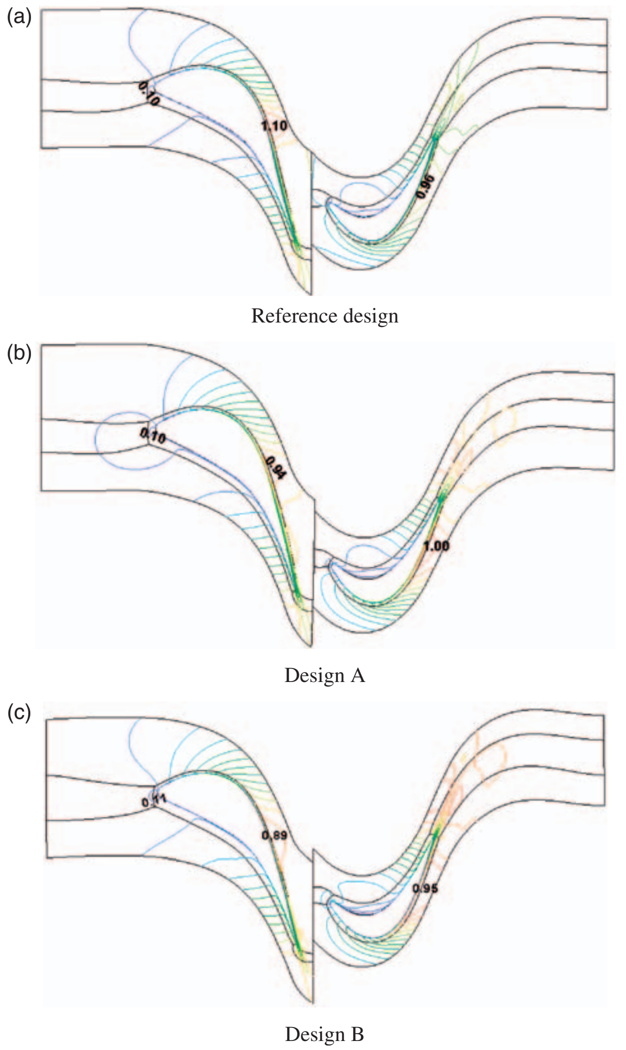

Fig. 12 Relative Mach number contours at the middle section: (a) reference design, (b) Design A, and (c) Design B

translation along the rotational direction and shows the feature of negative bowed structure; the rotor of Design B shows obvious translation along the direction opposite to the rotational direction and forms the design of leaning towards the pressure surface.

Figure 12 gives the relative Mach number contours at the middle section of the reference and optimized turbine stages. The maximum Mach numbers of the optimized stators are decreased from 1.10 to 0.94 (Design A) and 0.89 (Design B), respectively, which is caused by the decrease in the curvature on the suction surface of the stators. The pressure fluctuations of the optimized stators are effectively decreased in the passages. Compared with the reference rotor, the maximum Mach numbers of Design A rotor do not increase significantly, and the maximum Mach numbers of Design B rotor basically remain intact.

Figure 13 gives the total pressure loss coefficient distribution along the span at the 5 mm downstream

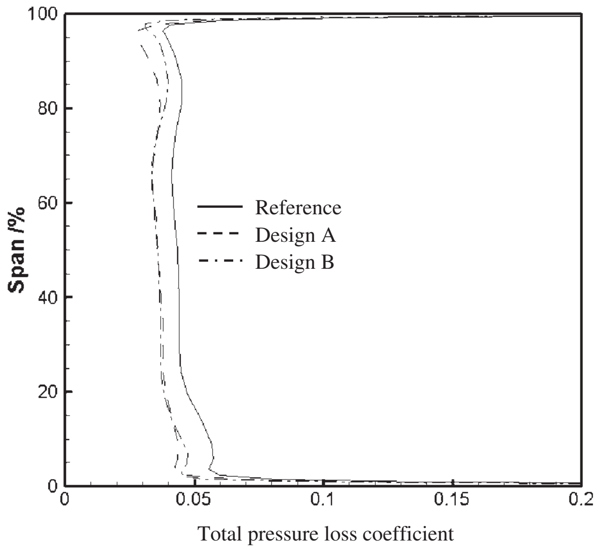

Fig. 13 Total pressure loss coefficient along the span

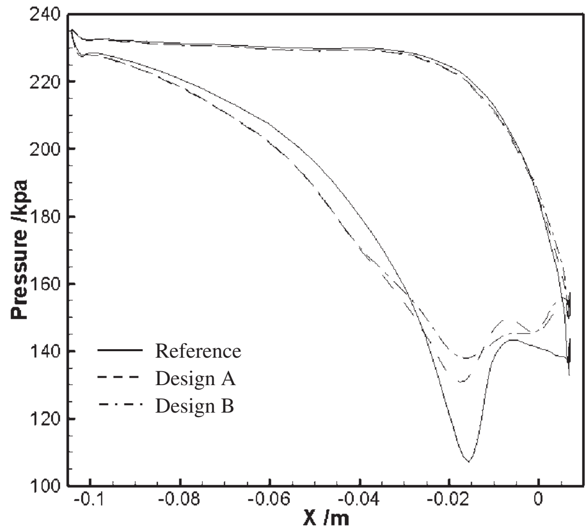

Fig. 14 Surface static pressure distribution at middle section of stator

the stator exit. The total pressure loss coefficient is defined as

$$\xi(\gamma) = \frac{P_0^t - P_1^t}{P_0^t - P_1^s} \tag{14}$$

where P_0^t denotes the total pressure of stator inlet, P_1^t the total pressure of stator outlet, and P_1^s the static pressure of stator outlet.

Let v_{av} denote the averaged axial velocity on dA. The pitchwise mass-averaged total pressure loss coefficient is defined as

$$\overline{\xi(\gamma)} = \int \xi(\gamma) \cdot \rho v_{av}\, \mathrm{d}A \Big/ \int \rho v_{ax}\, \mathrm{d}A \tag{15}$$

As can be seen from Fig. 13, compared with the reference design, the total pressure loss coefficient at the optimized stators outlet is obviously decreased along the whole span. This is mainly attributed to the obvious decrease in the sudden jump of the pressure on the suction surface throat area of the optimized stators (Fig. 14). Over 78–97 per cent of the span, the total pressure loss coefficient at the Design A stator outlet is evidently lower than that of Design B stator outlet.

Figure 15 gives the loss coefficient of the turbine stage rotor along the span. Over 10–95 per cent of the span, the loss coefficient of optimized rotors is obviously lower than that of the reference rotor. From the blade root to 10 per cent of the span, the loss coefficient of Design A rotor is higher than that of Design B rotor. This is because the negatively bowed structure of Design A rotor suppresses the development of the passage vortex towards the middle span and increases the loss at the rotor root. At the same time, the loss coefficient of Design A rotor is slightly lower than that of Design B rotor at the area close to the middle span. In addition, the distributions of the loss coefficients of Design A and Design B rotors look more uniform along the span.

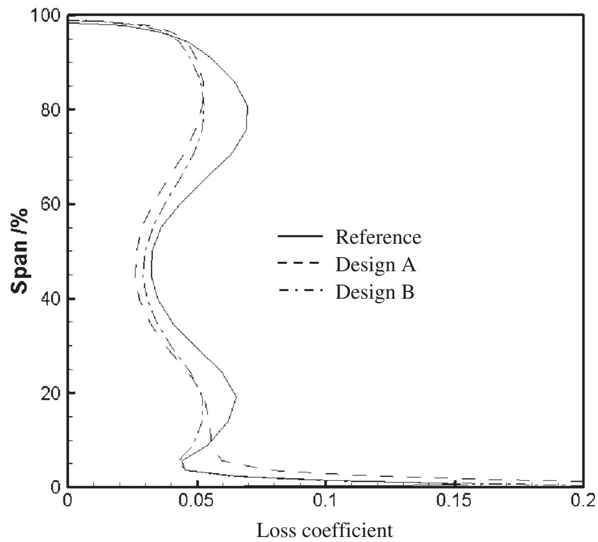

Fig. 15 Loss coefficient of the turbine stage rotor along the span

Figure 16 gives the mass flow of the turbine stage rotor along the span at the 10 mm downstream the rotor exit. As can be seen from this figure, the mass flow distributions along the span of both the reference design and Design A are very close. This also shows that the optimization of the turbine stage is different from the optimization of the single-row cascade, as the negative bow of the single-row cascade usually has a major influence on the mass flow distribution. From 7 per cent to 32 per cent of the span, the mass flow of Design B is higher than that of the reference design. From 32 per cent to 86 per cent of the span, the mass flow of Design B decreases compared with that of the reference design. It is because the lean of the rotor towards the pressure surface pushes the fluid from the top to the bottom.

Figure 17 shows the entropy production contours in the section 50 mm downstream the rotor of the reference and optimized turbine stages. The maximum entropy production of reference rotor outlet is 30.1 J/(kg · K) in the upper passage. However, the maximum entropy production of Design A rotor outlet is reduced to 26.2 J/(kg · K), and the maximum entropy production of Design B rotor outlet is decreased to 25.2 J/(kg · K) after the optimization. The maximum entropy production of the reference rotor outlet is 37.7 J/(kg · K) in the lower passage. After the optimization, the maximum entropy productions of Design A and Design B rotor outlets are reduced to 33.3 and 34.1 J/(kg · K), respectively. The analysis indicates that the flow losses of optimized turbine stages are obviously decreased in the passages. In addition, the ranges of the high-loss area at the optimized rotors outlet are also significantly reduced.

Figure 18 compares the isentropic efficiency at the grid outlet of the reference and optimized designs along the span. Over 6–95 per cent of the span, the

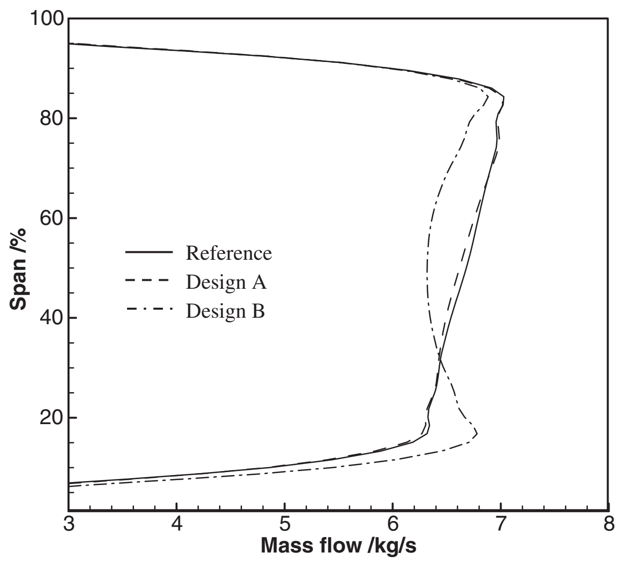

Fig. 16 Mass flow of the turbine stage rotor along the span

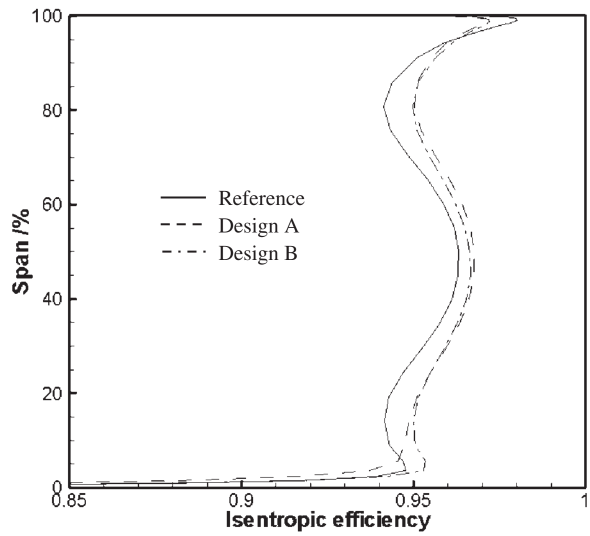

Fig. 18 Isentropic efficiency at the grid outlet along the span

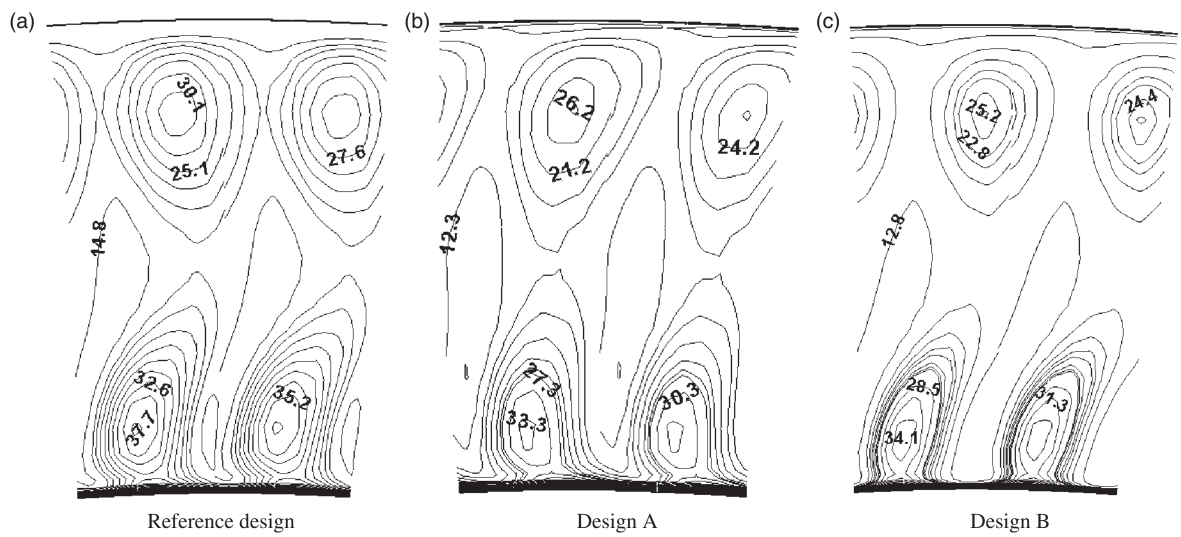

Fig. 17 Entropy production contours in the section 50 mm behind the rotor: (a) reference design, (b) Design A, and (c) Design B

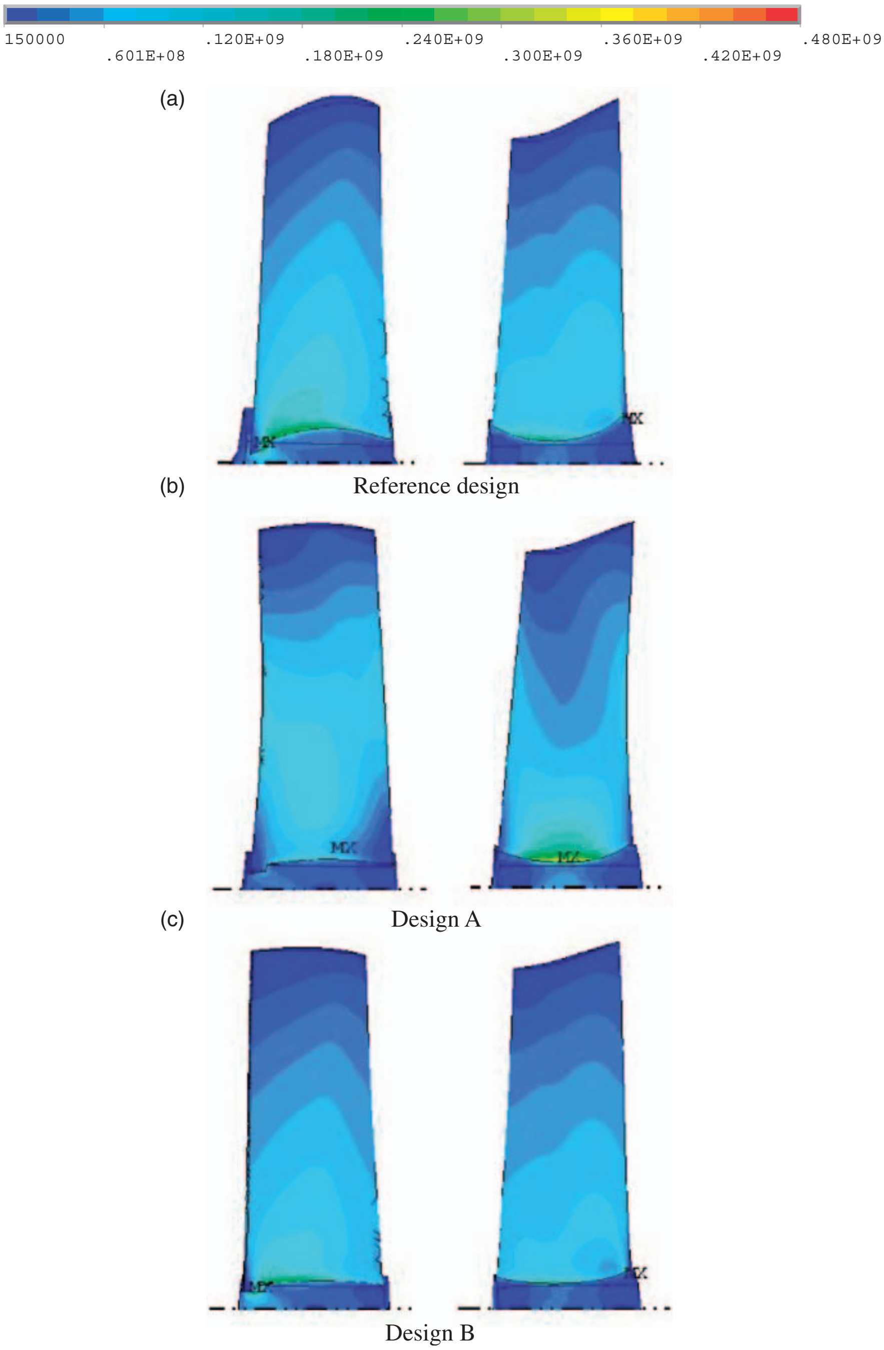

Fig. 19 Von Mises stress distribution in rotor pressure (left) and suction (right) surfaces: (a) reference design, (b) Design A, and (c) Design B

isentropic efficiency of the optimized turbine stages is evidently higher than that of the reference turbine stage, indicating that the aerodynamic performances of the optimized turbine stages are obviously improved. From the blade root to 6 per cent of the span, the isentropic efficiency of Design A is lower than that of the reference design.

Figure 19 compares the von Mises stress distributions of the reference, Design A, and Design B rotors. The maximum stresses of the reference and Design B rotors are located close to the front of the suction-side surface in the blade root, and the maximum stress of Design A rotor is located close to the middle of the suction-side surface of the joint between the blade surfaces and the blade base. Compared with the reference and Design B rotors, a higher stress distribution appears in the middle region of the pressure surface of the Design A, due to the negative bowed structure of the Design A. The von Mises stress distribution of Design B rotor is similar to that of the reference rotor. However, the range of the high-stress area of Design B rotor is obviously decreased. This

Table 5 Performances comparison

Parameters	Reference	Design A	Design B
Isentropic efficiency (%)	94.93	95.50	95.48
Increment (%)	0	0.57	0.55
Maximum stress (MPa)	479.6	420.2	355.5
Relative increment (%)	0	12.4	25.9
Mass flow (kg/s)	125.50	126.95	126.73
	650.3	642.6	655.9
	1099.6	1047.4	1099.9
	1644.7	1766.4	1666.9
	2166.1	2204.1	2201.5
The first ten vibration	3300.2	3314.2	3309.1
frequencies (Hz)	3583.8	3733.7	3624.9
	4522.5	4621.5	4513.8
	4988.3	5209.0	5021.1
	5109.3	5305.8	5157.9
	6216.7	6224.7	6266.8

may be due to the fact that the thickness of the root section of Design B rotor increases (Fig. 11(a)) and Design B rotor leans towards the suction surface. Considering the stress distribution and the maximum stress (Table5), Design B rotor is found to be better than the reference and Design A rotors. The efficiency of Design B is slightly lower than that of Design A. In the future study, the blade lifetime will be taken into account. If the Design A rotor has a computed lifetime still longer than that of the Design B rotor, Design A rotor is better than the reference and Design B rotors, with consideration of both efficiency and lifetime.

Table 5 compares the performances of the reference and optimized turbine stages. The isentropic efficiency of Design A increases by 0.57 per cent, and the maximum stress of Design A rotor relatively decreases by 12.4 per cent compared with those of the reference design. The isentropic efficiency of Design B is 0.55 per cent higher than that of the reference design, and the maximum stress of Design B has its maximum stress decreased by 25.9 per cent. The mass flowrates and the first ten vibration frequencies of Designs A and B meet the constraint requirements. Isentropic efficiency of Design B decreased by 0.02 per cent, while its maximum stress decreased by 15.4 per cent compared with that of Design A.

6 CONCLUSIONS

1. A new optimization algorithm named as SMODE is proposed, and a new constraint-handling method based on multi-objective optimization concept is used for constraint handling. The tests of the multi-constraints and multi-objective problems indicate that the presented SMODE can effectively solve the multi-constraint and multi-objective problems.
2. Applying SMODE as an optimizer and integrating 3D blade modelling method based on non-uniform B-spline, load-fitting transfer algorithm in parameter space, 3D Navier–Stokes solution technique, and finite element analysis method, an automated multi-objective and MDO method of axial turbomachinery blades is proposed.
3. The proposed method was applied to the MDO process of a transonic turbine stage in order to maximize the isentropic efficiency and minimize the maximum stress in the rotor with constraints on mass flowrate and dynamic frequencies. After the optimization, seven Pareto solutions are obtained. Results of the analysis of Designs A and B indicate that the aerodynamic and mechanic performances of the optimized designs are significantly improved. The results also demonstrate that the presented method has good performance and is adaptable to the MDO of turbomachinery blades.
4. The isentropic efficiency of Design B decreased by only 0.02 per cent, but Design B obtained a decrease in the profit of the maximum stress by 15.4 per cent compared with those of Design A. Provided that the requirement of strength is higher, Design B is recommended as the first choice for the designer. This reflects the advantage of the multi-objective and MDO method that takes the maximum stress as the objective function.

FUNDING

This work was supported by the National Natural Science Foundation of China [Grant Number 51106123] and the Specialized Research Fund for the Doctoral Program of Higher Education of China [Grant Number 20100201120010].

REFERFENCES

1 **Pierret, S., and Van den Braembussche, R.** Turbomachinery blade design using a Navier–Stokes solver and artificial neural network. *J Turbomach.*, 1999, **121**(2), 326–332.

2 **Oyama, A., Liou, M.,** and **Obayashi, S.** Transonic axial-flow blade shape optimization using evolutionary algorithm and three-dimensional Navier–Stokes Solver. AIAA paper no. 2002-5642, 2002.

3 **Benini, E.** Three-dimensional multi-objective design optimization of a transonic compressor rotor. *J. Propul. Power*, 2004, **20**(3), 559–565.

4 **Moroz, L., Yuri, G., Leonid, R.,** and **Petr, P.** Methods and tools for multidisciplinary optimization of axial turbine stages with relatively long blades. ASME paper no. GT2004-53000, 2004.

5 **Verstraete, T., Alsalihi, R. A.,** and **Van de Braembussche, R. A.** Multidisciplinary optimization of a radial compressor for micro gas turbine application. ASME paper no. GT-2007-27484, 2007.

6 **Pierret, S., Filomeno Coelho, R.,** and **Kato, H.** Multidisciplinary and multiple operating points shape optimization of tree-dimensional compressor blades. *Struct. Multidisc. Optim.*, 2007, **33**, 61–70.
7 **Siller, U., VoB, C.,** and **Nicke, E.** Automated multidisciplinary optimization of a transonic axial compressor. In Proceedings of the 47th AIAA Aerospace Sciences Meeting Including the New Horizons Forum and Aerospace Exposition, Orlando, Florida, 5–8 January 2009, AIAA paper no. 2009-863, pp. 092407.1–12 (American Institute of Aeronautics and Astronautics, Washington, District of Columbia).
8 **Storn, R.** and **Price, K.** Differential evolution - a simple and efficient adaptive scheme for global optimization over continuous space. Technical Report, International Computer Science Institute, Berkley, 1995.
9 **Storn, R.** and **Price, K.** Differential evolution - a simple and efficient heuristic for global optimization over continuous spaces. *J. Glob. Optim.*, 1997, **11**(4), 341–359.
10 **Madavan, N. K.** Multi-objective optimization using a Pareto differential evolution approach. In IEEE Proceedings of the Congress on *Evolutionary computation*, Honolulu, Hawaii, 12–17 May 2002, pp. 1145–1150, paper no. CEC.2002.1004404 (IEEE Service Center, Piscataway, New Jersey).
11 **Li, H.** and **Zhang Q. F.** A multi-objective differential evolution based on decomposition for multi-objective optimization with variable linkages. In Proceedings of the Parallel Problem Solving from Nature, PPSN IX, Reykjavik, Iceland, 9–13 September 2006, LNCS 4193, pp. 583–592 (Springer-Verlag, Berlin).
12 **Zamuda, A., Brest, J., Boskovic, B.,** and **Zumer, V.** Differential evolution for multi-objective optimization with self adaptation. In IEEE. Proceedings of the Congress *on Evolutionary computation*, Singapore, 25–28 September 2007, pp. 3617–3624 (IEEE Press, Piscataway, New Jersey).
13 **Beyer, H. G.** and **Schwefel, H. P.** Evolution strategies – a comprehensive introduction. *Nat. Comput.*, 2002, **1**, 3–52.
14 **Li, H.** and **Zhang, Q.** Multi-objective optimization problems with complicated Pareto sets, MODE/D and NSGA-II. *IEEE Trans. Evol. Comput.*, 2009, **13**(2), 284–302.
15 **Deb, K.** An efficient constraint-handling method for genetic algorithms. *Comput. Meth. Appl. Mech. Eng.*, 2000, **186**(2–4), 311–338.
16 **Coello, C. A. C.** Constraint-handling using an evolutionary multi-objective optimization technique. *Civil. Eng. Environ. Syst.*, 2000, **17**(4), 319–346.
17 **Oyama, A., Shimoyama, K.,** and **Fujii, K.** New constraint-handling method for multi-objective multi-constraint evolutionary optimization and its application to space plane design. In Proceedings of the Optimization and Control with Applications to Industrial and Societal Problems. EUROGEN 2005 (Eds R. Schilling, W. Haase, J. Periaux, H. Baier, and G. Bugeda), Munich, Germany, 12–14 September 2005, pp. 416–428.
18 **Jimenez, F.** and **Verdegay, J. L.** Evolutionary techniques for constrained optimization problems. In Proceedings of the 7th European Congress on Intelligent Techniques and Soft Computing, Aachen, Germany, 14–19 September 1999.
19 NUMECA International. NUMECA FINE/Turbo Version 8.2-1, NUMECA International, Belgium, 2007.
20 ANSYS. *ANSYS theory manual*, ANSYS 11.0 Help System, 2007 (ANSYS, Canonsburg).
21 **Li, L. Z., Lu, Z. Z., Wang, J. C.,** and **Yue, Z. F.** Turbine blade temperature transfer using the load surface method. *Comput.-Aided Des.*, 2007, **39**, 494–505.
22 **Arnone, A., Marconcini, M., Pacciani, R., Schipani, C.,** and **Spano, E.** Numerical investigation of airfoil clocking in a three-stage low-pressure turbine. *J. Turbomach.*, 2002, **124**(1), 61–68.
23 **Benini, E.** and **Toffolo, A.** Innovative procedure to minimize multi-row compressor blade dynamic loading using rotor-stator interaction optimization. *Proc. IMechE, Part A: J. Power Energy*, 2007, **221**(1), 59–66.

APPENDIX

Notation

CR	crossover factor $CR \in (01.0]$
f_i	ith objective function
$f_{j,vib}$	jth vibration frequency (Hz)
$f_{i,forb}^{low}$	lower limit of the ith forbidden frequency range (Hz)
$f_{i,forb}^{up}$	upper limit of the ith forbidden frequency range (Hz)
F	scaling factor $F \in (01.0]$
F_{obj}	objective function
g_i	ith constraint
h_0	total enthalpy (J/kg)
LOW_j	lower bound of the jth decision variable
m	mass flowrate (kg/s)
n_s	rotational speed of the rotor per second (r/s)
NP	population size
P_m	mutation rate
$randk$	randomized numbers $randk \in [0, 1]$
$randm$	randomized numbers $randm \in [0, 1]$
UP_j	upper bound of the jth decision variable
x_i	ith variable
$X_{j,i}$	jth individual of the generation i
Z_1	number of stator blades
η	distribution index
η_{is}	isentropic efficiency
$\sigma_{\max}$	maximum stress (Pa)

Subscripts

ref	reference design
1	inlet
2	outlet